INTERFEROMETRIC REDATUMING USING DIRECT-WAVEFIELD MODELING

T. A. Coimbra, D. F. Barrera P., J. Schleicher and A. Novais

email: *js@ime.unicamp.br*

keywords: *redatuming, interferometry, reciprocity, direct wave.*

ABSTRACT

Redatuming aims at correcting seismic data for effects of an acquisition at an irregular surface and for the effects of complex geological structures in the overburden and low velocity layer. Interferometric techniques can be used to relocate sources to positions where only receivers are available and have been used to move acquisition geometries to the ocean bottom or transform data between surface-seismic and vertical seismic profiles. By combining modeling with interferometry and correlating the modeled direct wavefield with seismic surface data, we can relocate the acquisition system to any datum in the subsurface to which the propagation of direct waves can be modeled with sufficient accuracy. In this way, we can carry the seismic acquisition geometry from the surface to geologic horizons of interest. Specifically, we show the derivation and approximation of the seismic interferometry equation, conveniently using Green's theorem for the Helmholtz equation with density variation. We demonstrate theoretically and numerically that reflections from deeper interfaces are repositioned with satisfactory accuracy.

INTRODUCTION

In recent years there has been a growing interest to improve petroleum exploration and processing of seismic data using interferometric techniques. Seismic interferometry is a technique based on optical physics. It allows the use of parts of the information contained in the seismic data that are not taken into account in conventional processing. Its basic principle allows us to generate new seismic responses or virtual sources where only receivers were placed (Wapenaar et al., 2010). In seismic exploration, authors like Claerbout (1968) and Scherbaum (1978) were the first to make use of interferometric techniques. Claerbout (1968) showed that the Green's function for reflections recorded at the Earth's surface could be obtained by the autocorrelation of the data generated by buried sources in a 1D medium, while Scherbaum (1978), using information of microquakes, constructed geological structure based on the properties of the Green's functions.

Interferometric redatuming techniques have been studied, e.g., by Xiao and Schuster (2006), Schuster and Zhou (2006), Dong et al. (2007), Lu et al. (2008), van der Neut et al. (2011) and many others. They attempt to use the techniques with the objective of improving the seismic sections and reducing the uncertainty in hydrocarbon exploration in regions of high structural and sedimentological complexity. The redatuming technique's principal applications are the correction of seismic data for effects of an acquisition at an irregular surface and for the effects of complex geological structures in the overburden and low velocity layer. The objective is to focus the seismic data processing at a specific subsurface region.

Interferometric redatuming can be used to relocate sources to positions where only receivers are available and allows to carry the seismic acquisitions from the surface to geologic horizons of interest. In this work, we correlate the modeled direct wavefield with seismic surface data to relocate the acquisition system to any datum in the subsurface to which the propagation of direct waves can be modeled with sufficient accuracy.

The derivation starts from a convenient approximation of the seismic interferometry equation using Green's theorem on the Helmholtz equation with density variation. It proceeds to the general redatuming equation and the specific approximation discussing the correlation of acquired seismic data with modeled direct waves. In the numerical results section, we apply the new redatuming method to synthetic surface data from a simple earth model in order to redatum sources and receivers to the ocean bottom.

METHOD

In this section we describe the basic theory of interferometry for acoustic media with density variation. We deduce the reciprocity theorem, interferometry principle and the Green's function approximation. We start at the Helmholtz equation for variable-density media, which is written as follows

$$\rho(x)\nabla\cdot\left[\frac{1}{\rho(x)}\nabla\hat{\psi}(x,\omega)\right]+\frac{\omega^2}{v^2(x)}\hat{\psi}(x,\omega)=-\hat{F}(x,\omega)\ . \tag{1}$$

Here, $\rho(x)$ is the variable density, $\hat{\psi}(x,\omega)$ is the pressure field, ω is the angular frequency, $v(x)$ is the wave velocity, and $F(x,\omega)$ is a source term.

In the particular case of a temporal and spatial point source at position x_A, i.e., when the source term $F(x,\omega)$ is given by a delta function $\delta(x-x_A)$, the pressure field is represented by the Green's function $\hat{G}(x,\omega;x_A)$, so that the Helmholtz equation reads

$$\rho(x)\nabla\cdot\left[\frac{1}{\rho(x)}\nabla\hat{G}(x,\omega;x_A)\right]+\frac{\omega^2}{v^2(x)}\hat{G}(x,\omega;x_A)=-\delta(x-x_A). \tag{2}$$

The basis for all seismic interferometry is Gauss's theorem, which relates an integral over a closed surface ∂E of an arbitrary vector field to an integral over the enclosed volume E of the divergence of the vector field. Choosing the vector field appropriately, this theorem can be written as (Green, 1828)

$$\oiint_{\partial E}\frac{1}{\rho(x)}(\hat{\psi}\nabla\hat{G}-\hat{G}\nabla\hat{\psi})\cdot\hat{n}dS=\iiint_{E}\nabla\cdot\left(\frac{1}{\rho(x)}\hat{\psi}\nabla\hat{G}-\frac{1}{\rho(x)}\hat{G}\nabla\hat{\psi}\right)dV, \tag{3}$$

where $\hat{n}$ is the unit vector normal to the surface ∂E pointing into the outward direction of the volume E.

Reciprocity theorem

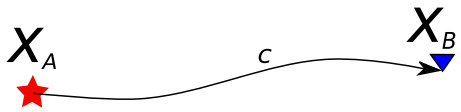

Figure 1: Sketch of a source at position x_A with a receiver at position x_B, where c is the representation of a wave path from x_A to x_B.

To derive the reciprocity theorem for variable-density media, we consider the situation in Figure 1. Upon the use of equation (3), we deduce the reciprocity theorem for wave propagation between points x_A and x_B. We start from equations (1) and (2). For simplicity, we write $\hat{\psi}=\hat{\psi}(x,\omega)$ and $\hat{G}_A=\hat{G}(x,\omega;x_A)$. Multiplying equation (1) by $\hat{G}_A$, we obtain

$$\rho(x)\hat{G}_A\nabla\cdot\left[\frac{1}{\rho(x)}\nabla\hat{\psi}\right]+\frac{\omega^2}{v^2(x)}\hat{G}_A\hat{\psi}=-\hat{F}(x,\omega)\hat{G}_A, \tag{4}$$

and multiplication of equation (2) by $\hat{\psi}$ yields

$$\rho(x)\hat{\psi}\nabla\cdot\left[\frac{1}{\rho(x)}\nabla\hat{G}_A\right]+\frac{\omega^2}{v^2(x)}\hat{\psi}\hat{G}_A=-\delta(x-x_A)\hat{\psi}. \tag{5}$$

Subtracting equations (4) and (5) after division by $\rho(x)$, integrating over an arbitrary volume E, and applying Green's theorem (3), we find

$$\oiint_{\partial E} \frac{1}{\rho(x)} \left(\hat{\psi} \nabla \hat{G}_A - \hat{G}_A \nabla \hat{\psi} \right) \cdot \hat{n} dS = \iiint_E \frac{1}{\rho(x)} \left[\hat{F}(x,\omega) \hat{G}_A - \delta(x - x_A) \hat{\psi} \right] dV. \tag{6}$$

Using the Sommerfeld radiation condition, is possible demonstrate that the left-hand-side integral of the above equation tends to zero when the radius of the closed surface tends to infinity, i.e.,

$$\lim_{r \to \infty} \oiint_{\partial E(r)} \frac{1}{\rho(x)} \left(\hat{\psi} \nabla \hat{G}_A - \hat{G}_A \nabla \hat{\psi} \right) \cdot \hat{n} dS = 0. \tag{7}$$

This results in the following equation for the solution to equation (1) at a point x_A,

$$\hat{\psi}(x_A, \omega) = \rho(x_A) \iiint_{\mathbb{R}^3} \frac{1}{\rho(x)} \hat{F}(x,\omega) \hat{G}_A dV. \tag{8}$$

Considering the source of equation (1) to be a point source at x_B, i.e., $\hat{F}(x,\omega) = \delta(x - x_B)$, we have

$$\hat{G}(x_A, \omega; x_B) = \rho(x_A) \iiint_{\mathbb{R}^3} \frac{1}{\rho(x)} \delta(x - x_B) \hat{G}(x, \omega; x_A) dV, \tag{9}$$

which results in the identity

$$\frac{\hat{G}(x_A, \omega; x_B)}{\rho(x_A)} = \frac{\hat{G}(x_B, \omega; x_A)}{\rho(x_B)}, \tag{10}$$

relating the Green's functions for propagation from x_A to x_B and from x_B to x_A. From equation (10), we see that the Green function between points x_A and x_B is not reciprocal, if the values of the densities at these points are different. However, a density-scaled Green's function (Bleistein et al., 2001) is reciprocal. This can be seen by multiplying each side of equation (10) by a density factor

$$\left[\frac{\hat{G}(x_A, \omega; x_B)}{\rho(x_A)} = \frac{\hat{G}(x_B, \omega; x_A)}{\rho(x_B)} \right] \sqrt{\rho(x_A)\rho(x_B)}\,, \tag{11}$$

which yields

$$\sqrt{\frac{\rho(x_B)}{\rho(x_A)}} \hat{G}(x_A, \omega; x_B) = \sqrt{\frac{\rho(x_A)}{\rho(x_B)}} \hat{G}(x_B, \omega; x_A)\,. \tag{12}$$

Let us define the density-scaled Green's function as

$$\hat{g}(x, \omega; x_s) = \sqrt{\frac{\rho(x_s)}{\rho(x)}} \hat{G}(x, \omega; x_s), \tag{13}$$

where x_s is the source position. Then, the original Green's function can be recovered from its density-scaled version by

$$\hat{G}(x, \omega; x_s) = \sqrt{\frac{\rho(x)}{\rho(x_s)}} \hat{g}(x, \omega; x_s). \tag{14}$$

Note that in the case of constant density the density-scaled Green's function $\hat{g}(x, \omega; x_s)$ reduces to the Green's function $\hat{G}(x, \omega; x_s)$ itself.

With definition (13), the reciprocity relation (12) reads

$$\hat{g}(x_A, \omega; x_B) = \hat{g}(x_B, \omega; x_A). \tag{15}$$

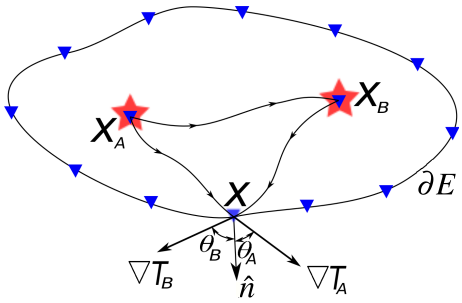

Figure 2: Sketch of two sources at positions x_A and x_B inside a volume E with receivers along the closed surface ∂E of E. Indicated at position x are the propagation directions of the incoming waves from x_A and x_B, and their angles θ_A and θ_B with respect to the unit normal vector $\hat{n}$ to the surface.

Interferometry

Let us now review the basic interferometry equation (see, e.g., Wapenaar et al., 2010). We consider the case where we have a closed surface with receivers located on it. Inside the enclosed volume, we have two sources located in positions x_A and x_B (see Figure 2).

We start from the complex conjugate of the Helmholtz equation (1) with a point source at x_B. With the simplified notation $G_B^* = \hat{G}^*(x, \omega; x_B)$, where the asterisk denotes the complex conjugate, the corresponding equation reads

$$\rho(x)\nabla \cdot \left[\frac{1}{\rho(x)}\nabla \hat{G}_B^*\right] + \frac{\omega^2}{v^2(x)}\hat{G}_B^* = -\delta(x - x_B). \tag{16}$$

Multiplying equations (2) and (16) by $\hat{G}_B^*$ and $\hat{G}_A$, respectively, and subtracting the results after division by $\rho(x)$, we find

$$\nabla \cdot \left[\frac{1}{\rho(x)}\left(\hat{G}_A \nabla \hat{G}_B^* - \hat{G}_B^* \nabla \hat{G}_A\right)\right] = \frac{1}{\rho(x)}\left(\delta_A \hat{G}_B^* - \delta_B \hat{G}_A\right). \tag{17}$$

Integration over an arbitrary volume E, application of Green's theorem (3), and consideration of the reciprocity relation (10) leads to

$$\oiint_{\partial E} \frac{1}{\rho(x)}\left(\hat{G}_A \nabla \hat{G}_B^* - \hat{G}_B^* \nabla \hat{G}_A\right) \cdot \hat{n} dS = \frac{-2i}{\rho(x_B)} \mathrm{Im}\left[\hat{G}(x_B, \omega; x_A)\right]. \tag{18}$$

This is the fundamental relationship for all interferometry techniques, because it proves that the Green's function of the propagation from x_A to x_B can be obtained with information about the wavefield propagating from x_A and from x_B to (all) receivers on the closed surface. This only is possible if x_A and x_B are located inside the closed surface.

Green's function approximation

For practical purposes, equation (18) is inadequate, because it is extremely rare that data on closed surfaces are available. Moreover, the Green's functions' gradients generally are unknown. Therefore, the quantities in equation (18) need to be approximated by practically available data. For the following considerations, we refer again to Figure 2.

In the high-frequency situation, we can replace the Green's functions by their asymptotic WKBJ approximations,

$$\hat{G}(x, \omega; x_s) \approx L(x; x_s) \exp\left[-i\omega T(x; x_s)\right]. \tag{19}$$

There, T is the traveltime from x_s to x which satisfies the eikonal equation $\|\nabla T(x; x_s)\|^2 = \frac{1}{v^2(x)}$ and $L(x; x_s)$ is the amplitude, principally determined by geometrical spreading. Also in high-frequency approximation, the Green's function's gradient can be approximated by

$$\nabla \hat{G}(x, \omega; x_s) \approx -i\omega \hat{G}(x, \omega; x_s) \nabla T. \tag{20}$$

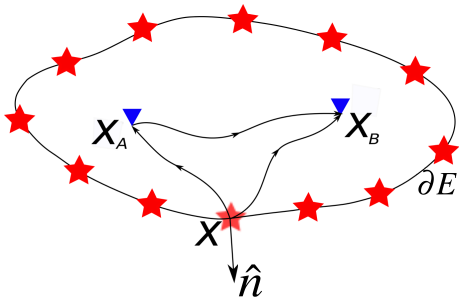

Figure 3: Sketch of two receivers inside a volume E at positions x_A and x_B and sources along the closed surface ∂E of E.

The product of the traveltime gradient with the surface normal yields $\nabla T \cdot \hat{n} = \cos\theta / v(x)$, where θ is the incidence angle of the wavefield under consideration. Thus, substituting equations (19) and (20) in (18) and defining the obliquity factor

$$\Theta(x; x_A, x_B) = \frac{\cos\theta_A + \cos\theta_B}{2v(x)} \,, \tag{21}$$

we obtain

$$-\omega\rho(x_B) \oiint_{\partial E} \frac{1}{\rho(x)} \hat{G}_A \hat{G}_B^* \Theta(x; x_A, x_B) dS \approx \text{Im}\left[\hat{G}(x_B, \omega; x_A)\right] . \tag{22}$$

If the surface is sufficiently far away from the points x_A and x_B, the angles θ_A and θ_B between the ray paths and the surface normal approximately vanish, so that $\Theta \approx \frac{1}{v(x)}$. Thus, in far-field approximation, we can write

$$-\omega\rho(x_B) \oiint_{\partial E} \frac{1}{\rho(x)v(x)} \hat{G}_A \hat{G}_B^* dS \approx \text{Im}\left[\hat{G}(x_B, \omega; x_A)\right] . \tag{23}$$

Considering equations (13) and (15), we can recast equation (23) into the form

$$-\omega \oiint_{\partial E} \frac{1}{v(x)} \hat{g}(x_A, \omega, x) \hat{g}^*(x_B, \omega; x) dS \approx \text{Im}\left[\hat{g}(x_A, \omega; x_B)\right] . \tag{24}$$

Equation (24) shows that the situation of Figure 2 can be exchanged for one where instead of sources inside the volume, there are receivers, and instead of receivers at the surface, there are sources. This is the reciprocity principle (see Figure 3).

Direct-wave redatuming

As the next step, we understand the surface ∂E in Figure 2 as divided into two surfaces α and γ (see Figure 4). The surface α contains the sources and receivers of a conventional seismic array, and γ is a surface part that is needed to close it.

We suppose that seismic data have been acquired for sources at points x_A and receivers along the seismic array at α, and that a velocity model is known for the medium between surface parts α and γ, so that the direct wave from all points x_B on the datum to all points x_A on α can be estimated by seismic modeling. We will show in this section that cross-correlation of this modeled direct waves with the seismic surface data allows to approximately redatum the acquisition array (sources and receivers) to reference datum $\partial\Sigma$.

The total Green's function for the wavefield at surface α can then be decomposed in a unique way as $\hat{G} = \hat{G}^i + \hat{G}^s$ (Bleistein et al., 2001), where $\hat{G}^i$ is the solution of the wave equation in the known reference medium and $\hat{G}^s$ is the difference to the complete solution in the true medium. For a point source at x_A, $\hat{G}^i_A = \hat{G}^i(x, \omega; x_A)$ must satisfy

$$\mathcal{L}_0 \hat{G}^i_A = -\delta(x - x_A), \tag{25}$$

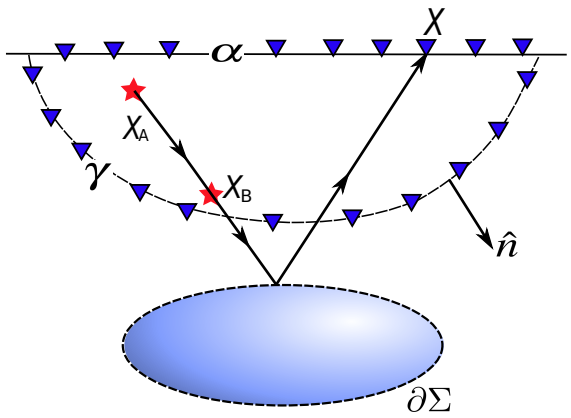

Figure 4: Sketch of the surface parts α and γ of ∂E including points x_A and x_B. Also shown is the surface $\partial\Sigma$ that is supposed to contain the unknown part of the medium.

where $\mathcal{L}_0$ is the Helmholtz operator for the reference medium, involving the density ρ_0 and and velocity v_0 instead of ρ and v.

The scattered field $\hat{G}^s_A = \hat{G}^s(x, \omega; x_A)$ must then satisfy a perturbed wave equation that can be written as

$$\mathcal{L}_0 \hat{G}^s_A = -\mathcal{V}(x) \left[\hat{G}^i_A + \hat{G}^s_A\right], \tag{26}$$

where $\mathcal{V}(x) = \mathcal{L} - \mathcal{L}_0$ is the difference between the perturbed and unperturbed Helmholtz operators, called the perturbation operator or scattering potential (Rodberg and Thaler, 1967).

In other words, the differences between the reference and true media are responsible for the existence of the scattering potential $\mathcal{V}$ and thus for the existence of the scattered wavefield $\hat{G}^s$. We assume that the region where the true medium is not known, i.e., where the perturbations between the reference medium and the true medium are located (indicated as $\partial\Sigma$ in Figure 4), is outside ∂E.

Using equations (25) and (26), we can set up an equation similar to equation (17). For this purpose, we multiply equation (26) with G^{i*}_B and the complex conjugate of equation (25) for a point source at x_B with G^s_A. Subtracting the results, we arrive at

$$\nabla \cdot \left[\frac{1}{\rho_0(x)} \left(\hat{G}^s_A \nabla \hat{G}^{i*}_B - \hat{G}^{i*}_B \nabla \hat{G}^s_A\right)\right] = \frac{1}{\rho_0(x)} \left(\hat{G}^{i*}_B \mathcal{V} \hat{G}_A - \delta_B \hat{G}^s_A\right). \tag{27}$$

After integration over a volume E containing x_B and application of Green's theorem, this yields

$$\oiint_{\alpha+\gamma} \frac{1}{\rho_0(x)} \left(\hat{G}^s_A \nabla \hat{G}^{i*}_B - \hat{G}^{i*}_B \nabla \hat{G}^s_A\right) \cdot \hat{n} dS = \iiint_E \frac{\hat{G}^{i*}_B \mathcal{V} \hat{G}_A}{\rho_0(x)} dV - \frac{\hat{G}^s_{BA}}{\rho_0(x_B)}, \tag{28}$$

where $\hat{G}^s_{BA} = \hat{G}^s(x_B, \omega; x_A)$. Here, we have written the closed surface ∂E as a sum of two parts, where α represents the portion where seismic data are available and γ the remaining portion.

Since we suppose that we know the medium perfectly well between x_A and x_B, we can choose the volume E such that $\mathcal{V} = \mathcal{L} - \mathcal{L}_0 = 0$ inside E (see figure 4). Thus, the volume integral in equation (28) vanishes. After high-frequency approximations analogous to equations (19) and (20), equation (28) therefore allows to approximately calculate the scattered field at x_B as

$$\hat{g}^s(x_B, \omega; x_A) \approx -2i\omega \iint_\alpha \hat{g}^s_A \hat{g}^{i*}_B \Theta(x; x_A, x_B) dS + \hat{I}_{BA}, \tag{29}$$

where $\Theta(x; x_A, x_B)$ is the obliquity factor defined in equation (21). As before, we will take $\Theta(x; x_A, x_B) \approx 1/v$ in the far-field approximation. Moreover, $\hat{I}_{BA}$ represents the integration over the surface portion γ where no seismic data are available. It denotes an undesired scattering term that gives

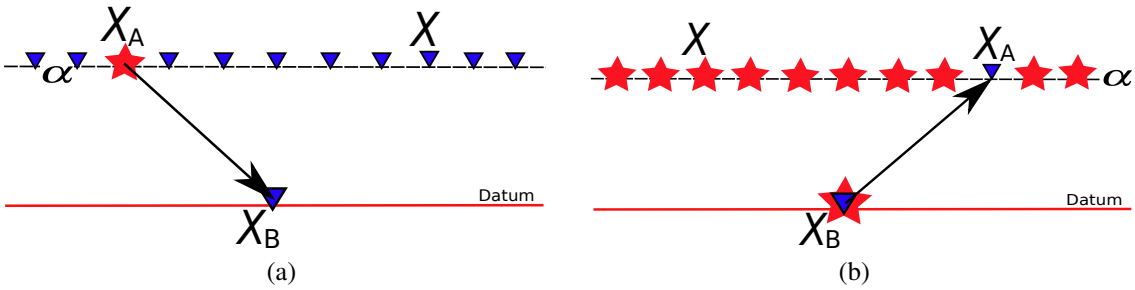

Figure 5: Sketch that shows the redatuming to a surface $\partial\Sigma$ in two steps: (a) receivers and (b) sources.

rise to spurious events. Its contribution will be negligible if the differences between the true and reference media are small.

Equation (29) is the principal theoretical result of this work. It states that it is possible to redatum surface data by means of interferometry using direct-wave modeling. This equation allows to obtain the Green's function at x_B for a point source at x_A by cross-correlation of the modeled direct wave in x_B with the acquired wavefield in x_A. To redatum the complete survey, equation (29) must be applied in two steps, first redatuming the receivers and then the sources (see Figure 5).

Scattering term To better understand the physical significance of the scattering term $\hat{I}_{BA}$ in equation (29), let us analyze it in more detail. For this purpose, we substitute the high-frequency approximations (19) and (20) to find

$$\begin{aligned}\hat{I}_{BA} &= \iint_{\gamma} \frac{\sqrt{\rho_0(x_A)\rho_0(x_B)}}{\rho_0(x)} \left(\hat{G}^s_A \nabla \hat{G}^{i*}_B - \hat{G}^{i*}_B \nabla \hat{G}^s_A\right) \cdot \hat{n} dS \\ &\approx -2i\omega \iint_{\gamma} \frac{\sqrt{\rho_0(x_A)\rho_0(x_B)}}{\rho_0(x)} L^s(x;x_A) L^i(x_B;x) \exp\left[i\omega(T_B - T_A)\right] \Theta(x;x_A,x_B) dS. \quad (30)\end{aligned}$$

This result demonstrates that the event described by integral $\hat{I}_{BA}$ is proportional to the amplitude L^s of the wave G^s_A that was scattered at the differences between the true medium and the one used for modeling of the direct wave. Thus, the smaller these differences are, the smaller will the spurious event become. In practice, the main contributions to equation (30) will be from the region below the datum.

More importantly, the stationary directions for integral (30) are those where the wavepath connects all three points x, x_A and x_B. For such wavepaths, the traveltime difference $T_B - T_A$ that governs the phase of integral (30) amounts to the traveltime T_{AB} of the direct wave between x_A and x_B. We will recognize in the numerical examples that the most important contribution of integral (30) appears at T_{AB} in the redatumed data.

NUMERICAL EXAMPLES

Synthetic data

To numerically validate redatuming interferometry equation (29), we applied it in a simple numerical experiments, considering a seismic marine acquisition. The model had a width of 1 km and a depth of 750 m. Synthetic seismic data were simulated considering three situations: (1) shots and receivers are located at the surface (Figure 6a), (2) shots are located at the surface and receivers at 350 m depth (Figure 6b) and (3) shots and receiver are located at 350 m depth (Figure 6c).

The seismic array at the surface consisted of 21 sources spaced at 40 m, located between coordinates 100 m and 900 m, and the same number of receivers for each shot, located at the same positions (Figure 6a). In the second experiment, we kept the same source array at the top surface, but used 21 receivers at 350 m depth at positions between 400 m and 600 m, spaced at 10 m (Figure 6b). Finally, in the third experiment we modeled synthetic data with the sources and receivers at the latter positions in depth (Figure 6c). The

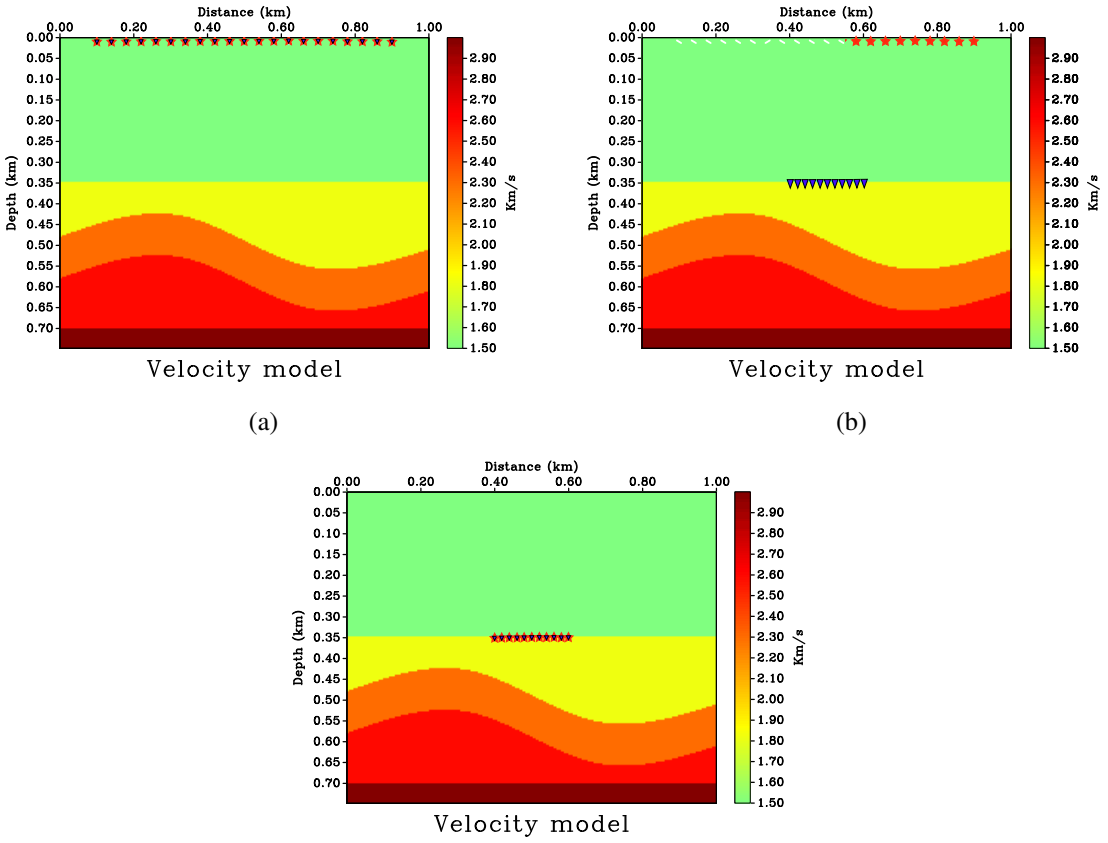

Figure 6: Modeling seismic data considering: (a) array of sources and receivers at the surface, (b) array of the sources at the surface and receivers at 350 m depth and (c) all array redatuming at 350 m depth.

wavelet used for the numerical modeling was a Ricker wavelet of 50 Hz peak frequency. To further simplify things we considered the density in all layers constant.

Interferometry results

The first step of redatuming the complete seismic array from the surface to the datum consists of redatuming the receivers, i.e., transforming the configuration of experiment 1 into that of experiment 2. Figure 7a compares the results of redatuming the receivers using equation (29) to the synthetic data directly modeled with the configuration of experiment 2 (Figure 7b).

To carry out the redatuming, we modeled all direct waves from all desired receiver positions at depth to all true source positions at the surface and crosscorrelated them with the surface data according to equation (29). Figure 7 shows the resulting common-receiver gathers at the new depth. We see that the kinematic properties of the data are nicely matched. While the overall amplitude features of the scattered waves are similar, we notice some differences.

For a more detailed analysis of the quality of the redatumed data, Figure 8 compares the redatumed trace at the center of both the source and receiver arrays to the modeled one. We see that all events are correctly positioned in time. Also, the amplitudes of the reflected events are comparable, while the waveforms are slightly altered. The main reason for the different amplitudes of the scattered waves is the approximation of the obliquity factor in equation (29). The principal difference between the traces is in the amplitude of the direct wave. The reason is that the direct wave is not recovered by equation (29). This event is actually described by the "scattering term" $\hat{I}_{BA}$, as explained above.

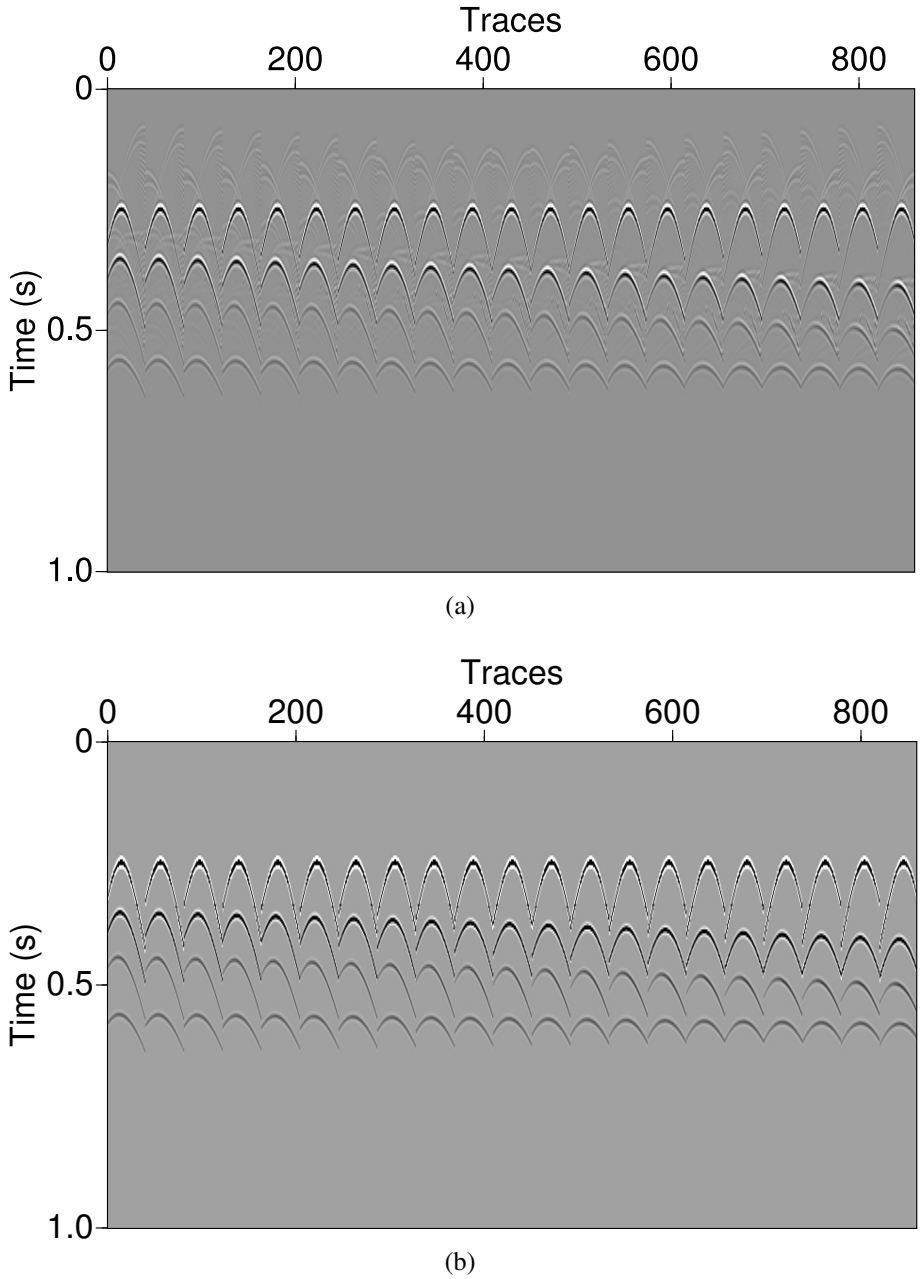

Figure 7: Redatuming using seismic direct-wave interferometry with the numerical model of Figure 6. (a) Redatumed data. (b) Modeled data.

The second step of full redatuming consists of repositioning the sources at depth, i.e., transforming the configuration of experiment 2 into that of experiment 3. We used both data sets of Figure 7 as an input to this second redatuming step. Figure 9 compares the resulting zero-offset sections to correspondingly modeled data at depth. We see that both the redatumed surface and ocean-bottom-receiver data (Figure 9a and b) resemble the modeled data (Figure 9c) quite nicely, with the three reflections events being correctly positioned. The two-step redatuming of the surface data introduces some additional noise and weak spurious events. These effects will probably reduce if more input data are available. Moreover, they can be mitigated by using appropriate tapers.

For better appreciation of the quality of the obtained results, Figure 10 shows a trace-to-trace compar-

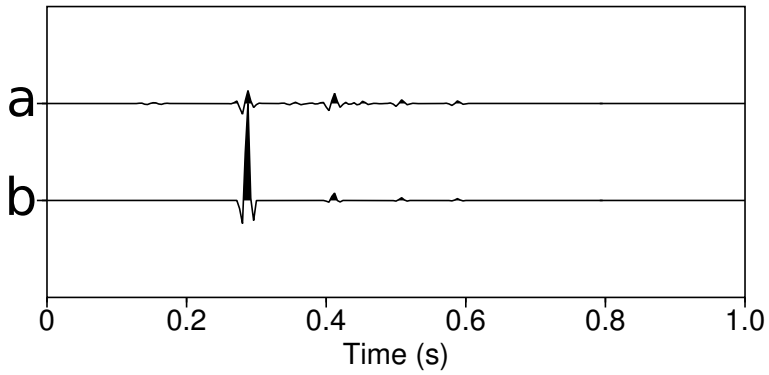

Figure 8: Comparison of trace no. 400 of Figures 7a and b. (a) Redatumed data. (b) Modeled data.

ison at midpoint coordinate 500 m. Figure 10 reveals that positions and relative amplitudes of the three reflections events are correctly recovered by both the one-step and two-step redatuming procedures. The interferometric wavelet changes by the correlations, and some noise becomes visible in the two-step result (Figure 10a), due to the low fold of the input data.

CONCLUSIONS

In this work, we have derived a new interferometric redatuming method combining acquired data with modeling of the direct wavefield in an approximately known overburden of the new datum. We have shown that a correlation of the modeled direct wavefield with seismic surface data permits to relocate the acquisition system to any datum in the subsurface to which the propagation of direct waves can be modeled with sufficient accuracy.

The derivation starts from a convenient approximation of the seismic interferometry equation using Green's theorem on the Helmholtz equation with density variation. It proceeds to the general redatuming equation and the specific approximation discussing the correlation of acquired seismic data with modeled direct waves. As with conventional redatuming, also interferometric redatuming proceeds in two steps, independently relocating sources and receivers to the new datum.

To investigate the feasibility of the new interferometric direct-wave redatuming, we have applied the method to synthetic surface data from a simple model in order to construct redatumed data for sources and receivers at the ocean bottom. Our numerical example demonstrates that the redatumed reflections events are repositioned correctly and keep the correct amplitude proportions as compared to data obtained from seismic modeling at the datum level.

Moreover, we have discussed the most important spurious event resulting from the approximate procedure. We have demonstrated theoretically and numerically that it will appear at the traveltime of the direct wave between the redatumed source and receiver positions. It will be the smaller the more accurate the model is that was used for the direct-wave modeling.

ACKNOWLEDGEMENTS

We are grateful to the Brazilian agencies CNPq and FINEP, as well as Petrobras and the sponsors of the Wave Inversion Technology (WIT) Consortium. The second author acknowledges a grant from the Santander Mobility Program.

REFERENCES

Bleistein, N., Cohen, J. K., and Jr., J. W. S. (2001). *Mathematics of Multidimensional Seismic Imaging, Migration, and Inversion*. Springer.

Claerbout, J. (1968). Synthesis of a layered medium from its acoustic transmission response. *Geophysics*, 33:264–269.

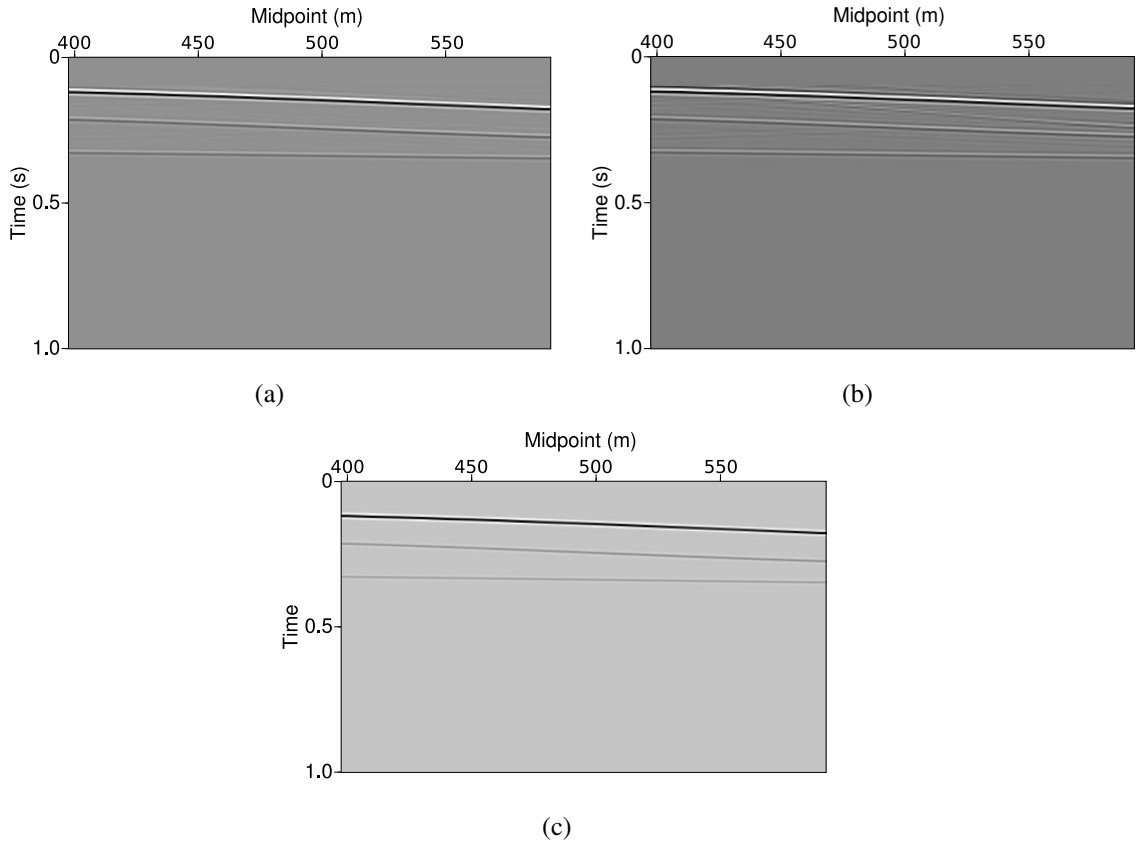

Figure 9: Zero-offset sections at the datum. (a) Two-step redatuming of the surface data, i.e., source redatuming of the data of Figure 7a. (b) One-step redatuming of the modeled ocean-bottom data of Figure 7b. (c) Modeled data.

Dong, S., Xiao, X., Luo, Y., and Schuster, G. (2007). 3D target-oriented reverse time datuming. *SEG Expanded Abstracts*, 26:2442–2445.

Green, G. (1828). *An eassy on the application of mathematical analysis to the theories of electricity and magnetism*. Privately published.

Lu, R., Willis, M., Chapman, X., Ajo-Franklin, J., and Toksöz, M. N. (2008). Redatuming through a salt canopy and target-oriented salt-flank imaging. *Geophysics*, 73:S63–S71.

Rodberg, L. S. and Thaler, R. M. (1967). Introduction to the quantum theory of scattering. *Academic Press*.

Scherbaum, F. (1978). Seismic imaging of the site response using microearthquake recordings. Part II. Aplication to the Swabian Jura, southwest Germany, seismic network. *Bulletin of Seismological Society of America*, 77:1924–1944.

Schuster, G. and Zhou, M. (2006). A theoretical overview of model- based and correlation-based redatuming methods. *Geophysics*, 71:SI103–SI110.

van der Neut, J., Thorbecke, J., Mehta, K., Slob, E., and Wapenaar, K. (2011). Controlled-source interferometric redatuming by crosscorrelation and multidimensional deconvolution in elastic media. *Geophysics*, 76:SA63–SA76.

Wapenaar, K., Draganov, D., Snieder, R., Campman, X., and Verdel, A. (2010). Tutorial on seismic interferometry: Part 1 - basic principles and applications. *Geophysics*, 75:75A195–75A209.

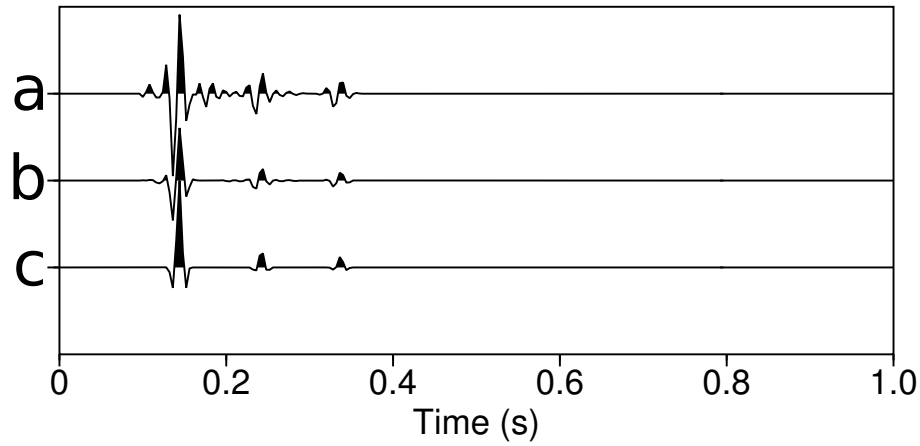

Figure 10: Comparison of the traces at position 500 m in Figure 9. (a) Two-step redatuming of surface data. (b) One-step redatuming of ocean-bottom data. (c) Modeled data.

Xiao, X. and Schuster, G. (2006). Redatuming CDP data below salt with VSP Green's function. *SEG Expanded Abstracts*, 25:3511–3515.